Quantifying effects of urban land-use patterns on flood regimes for a typical urbanized basin in eastern China

Mingming Song, Jianyun Zhang, Guodong Bian, Jie Wang and Guoqing Wang

ABSTRACT

Artificial adjustment and urbanization are key factors of global change and have significant influences on hydrological processes. This study focuses on the effects of urban land-use patterns on flood regimes in a typical urbanized basin in eastern China. Comprehensive assessments of urban land-use patterns were implemented on three levels: total imperviousness area (TIA) magnitude, landscape configuration and relative location in the basin. Hydrologic Engineering Center's Modeling System (HEC-HMS) was calibrated and validated using four groups of parameters associated with land-use conditions. Fourteen flood events were simulated based on 10 land-use scenarios with different land-use patterns. The results indicate that floods are closely associated with three landscape pattern indicators. First, over the past 20 years, the impermeability rate has increased from 3.92 to 17.48%, with the landscape pattern converted from extension growth form to fill-up growth form after 2003. Second, the average flood peak discharge increased by 80% due to impermeable surfaces expansion, with minor floods more sensitive to the expansion than major floods. Third, the contribution of imperviousness expansion to peak discharge in the inner basin is more remarkable than downstream of the river basin, with the landscape pattern metrics of TIA, arable land and forest land displaying strong correlations with flood characteristics.

Key words | flood regime, HEC-HMS, impervious surface, landscape pattern, scenario

Mingming Song
Jianyun Zhang
Guodong Bian
Jie Wang
Guoqing Wang (corresponding author)
State Key Laboratory of Hydrology-Water Resources and Hydraulic Engineering,
Nanjing Hydraulic Research Institute,
Nanjing 210009,
China;
Yangtze Institute for Conservation and Development,
Nanjing 210098,
China
and
Research Center for Climate Change,
Ministry of Water Resources,
Nanjing 210029,
China
E-mail: *gqwang@nhri.cn*

HIGHLIGHTS

- Comprehensive assessment of urban land use pattern were implemented through three levels.
- Hydrologic model was calibrated with varied parameters including land use change.
- Not only impervious area but the configuration was included in quantifying the urbanization effects.

INTRODUCTION

Hydrological cycles and their connection to changing human systems was one of the scientific themes in the new scientific decade 2013–2022 of the International Association of Hydrological Sciences (IAHS) (Montanari *et al.* 2013). Population growth and urban development have altered the natural environment, causing impermeable areas to expand dramatically (Cheng & Wang 2002; Fu & Weng 2016; Dadashpoor *et al.* 2019). This process exerts great influences on catchment hydrologic cycles by reducing precipitation interception, impeding infiltration water and creating overland flow. Coupled with increased frequency of extreme rainfall events as a result of climate change, the

doi: 10.2166/nh.2020.110

flood risk has increased and urban areas have become more vulnerable under the changing environment (Hollis 1975; Konrad & Booth 2005; Chen et al. 2009; Xu et al. 2010; Jiang et al. 2011; Debbage & Shepherd 2018; Oudin et al. 2018; Blum et al. 2020; Schober et al. 2020). To predict and manage flood risks associated with these changes, we need to quantify the causal links between impervious area change patterns and flood regimes.

Imperviousness is a critical environmental and hydrological indicator (Arnold & Gibbons 1996). It is often calculated as the area-weighted mean of the land-use categories. Mean imperviousness, also referred to as total imperviousness area (TIA), is often suggested to explain the hydrological impact of urbanization at basin scale (Oudin et al. 2018). Many researchers have analyzed the relationship between hydrological indicators and impervious area expansion. Chen et al. (2016) quantified urbanization impacts on surface runoff at a nation scale and found that 3.3 billion cubic meters of average annual runoff was gained due to urbanization for the decade 2001–2011. Cheng & Wang (2002) used a linear reservoir model in Taiwan's Wu-Tu river and found that the peak flow increased by 27% and the time to peak decreased by 4 hours while the impervious area ratio increased from 4.78 to 10.44%. Lee & Heaney (2003) evaluated the long-term impacts from an apartment area in Miami and found that the directly connected impervious area, which covered 44% of the catchment, contributed 72% of the total runoff volume over 52 years. Meanwhile, Hammer (1972) analyzed the relationships between increases in channel cross-sectional area and detailed land-use data in 78 small watersheds near Philadelphia and found important differences between the effects of various types of land use.

The effects of land use with different imperviousness levels on hydrological cycles have been extensively documented. Less analysis has focused on the flood responses to the changes of urban land-use pattern: spatial configuration of urban area and its relative location within a basin (Hammer 1972; Poff et al. 1997; Lee & Heaney 2003; Defries & Eshleman 2004; Hall et al. 2014; Kim & Park 2016; Debbage & Shepherd 2018).

Some researchers have used mathematical methods based on hydrologic and geographic records to quantify the relationship between impervious surface patterns and hydrological systems. For example, Debbage & Shepherd (2018) used variance tests, bivariate correlations, and multivariate regression models to quantify the relationship between urban spatial metrics and streamflow characteristics based on 119 watersheds. Oudin et al. (2018) gathered a sample of 142 catchments, and used regression analysis and urban landscape pattern metrics to interpret the divergent impacts of urban spread on flow regimes. Alberti et al. (2007) correlated changes in ecological conditions in 42 sub-basins with four urban pattern variables: land-use intensity, land cover composition, landscape configuration, and connectivity of the impervious area. Significant relationships were found between patterns of urban development and changes to aquatic ecosystems.

The hydrological model is another approach to quantify the urban landscape pattern effects. It can simulate the flow regime change based on scenario simulation, with less need for extensive hydrological data. Mejia & Moglen (2010) used an event-based model and scenarios typifying extreme cases of sprawl type and clustered development to examine the impacts of the impervious pattern. Zhou et al. (2013) studied the hydrological response to urbanization at different spatio-temporal scales by coupling the CLUE-S and the SWAT model in the Yangtze River Delta region and found that changes of hydrological fluxes were more remarkable in the suburban basin with greater urban growth than in rural sub-basins. Distributed hydrological models based on physical characteristics and land-use conditions have been proved to be effective tools in quantifying the urbanization effects on flood regimes. The distributed models, such as SWMM, SWAT, VIC, MIKE SHE and HEC-HMS, were widely used to simulate the hydrologic process. Of these, HEC-HMS (Hydrologic Engineering Center's Modeling System), which was developed by the U.S. Army Corps of Engineers, can be adapted to large-scale regions and basins with two outlets. Knebl et al. (2005) developed a framework for regional scale flood modeling which integrates NEXRAD level III rainfall, GIS, and a hydrological model (HEC-HMS/RAS). Oleyiblo (2010) used the HEC-HMS model and examined the model's capability and suitability for flood forecasting in catchments. Du et al. (2012) used CA-MARKOV to contribute several urbanization scenarios, coupling with the HEC-HMS model to examine the effects of urbanization on annual runoff and flood events. Gao et al. (2017) applied the HEC-HMS model in the Qinhuai

River basin to estimate the effects of urbanization on hydrological processes of the urban agglomeration polders. It is worth noting that the calibration methods used in HEC-HMS simulations were mostly based on one set of parameters. Most of these studies focused on basins with less impact of urbanization or had a shorter time span. However, for basins with dramatic urbanization during a long time span, a proper calibration method considering land-use changes should be further explored.

This study proposed a framework that integrates the impervious landscape pattern and HEC-HMS model. Urban land-use patterns were comprehensively assessed through three levels: the magnitude of TIA, landscape configuration and relative location in the basin. HEC-HMS was calibrated and validated using parameters associated with land-use conditions. Different land-use pattern scenarios were simulated to estimate the effects of urbanization on flood regimes. The specific objectives of this study are to: (1) quantify the effects of TIA magnitude on flood regimes through simulating the flood process under different TIA levels; (2) determine the impacts of urbanization relative location on flood flow behavior; and (3) quantify the effects of impervious area composite structure on flood regimes through investigating the relationship between landscape pattern metrics and flood characteristics.

STUDY AREA AND DATA

Description of Qinhuai River basin

The study area, located in the southwest of Jiangsu province, extends between 118°39′ and 119°19′E, 31°34′ and 32°10′N. The drainage area is 2,631 km^2. The whole basin was divided into three districts based on administrative boundaries: Nanjing-Jiangning (NJ + JN) district, Lishui (LS) district, and Jurong (JR) district.

The Jurong River and the Lishui River, two main tributaries on the upper Qinhuai River, converge from the north and south edges respectively to the center of the basin and become the main stream of the Qinhuai River near the Qianhancunqin (QHCQ) hydrometric station. The main stream is 36.6 km long and diverts near the DS rain gauge in Jiangning district. The east tributary flows to the north and converges into the Yangtze River through the Wudingmen outlet (WDM). The west tributary flows into the Yangtze River through the Qinhuai New River outlet (QHXH).

The elevation of the study area ranges from 0 to 417 m. The center and northwest of the fan-shaped basin are low while the rest of the area is relatively high. The river basin has been influenced by a subtropical monsoon climate. The average temperature is 15 °C and the annual average rainfall is 1,119 mm. The rainy season of the drainage area is fairly long and mainly includes three periods: April to mid-May, late June to early July and August to September. The average rainfall in the three rainy periods is 190, 348 and 205 mm, respectively.

The sub-basin of the Jurong tributary is monitored by the Qianhancunju (QHCJ) hydrometric station. The total upper river scope of the Jurong tributary sub-basin and Lishui tributary sub-basin is monitored by the QHCQ hydrometric station. The two downstream tributaries converge into the Yangtze River through two outlets. They are monitored by two outlet hydrometric stations: WDM and QHXH. The river system and gauge location of the Qinhuai River basin is shown in Figure 1.

Data and framework

Figure 2 shows the framework of hydrological response to changes in TIA. The land-use data and administrative boundary data were used to calculate the landscape pattern metrics of TIA and construct the urbanization scenarios. Land-use data, DEM, soil data and hydrological data were applied to calibrate and validate the HEC-HMS model. Based on the simulation of 14 flood events under different urbanization scenarios, an integrative analysis on hydrological responses was conducted.

METHODS

TIA information extraction

TIA is the percentage of the impervious surface area to the total catchment area. The TIA information was extracted from Landsat images for the period 1994–2013, and the quality of the images was relatively high. Rotation Forest,

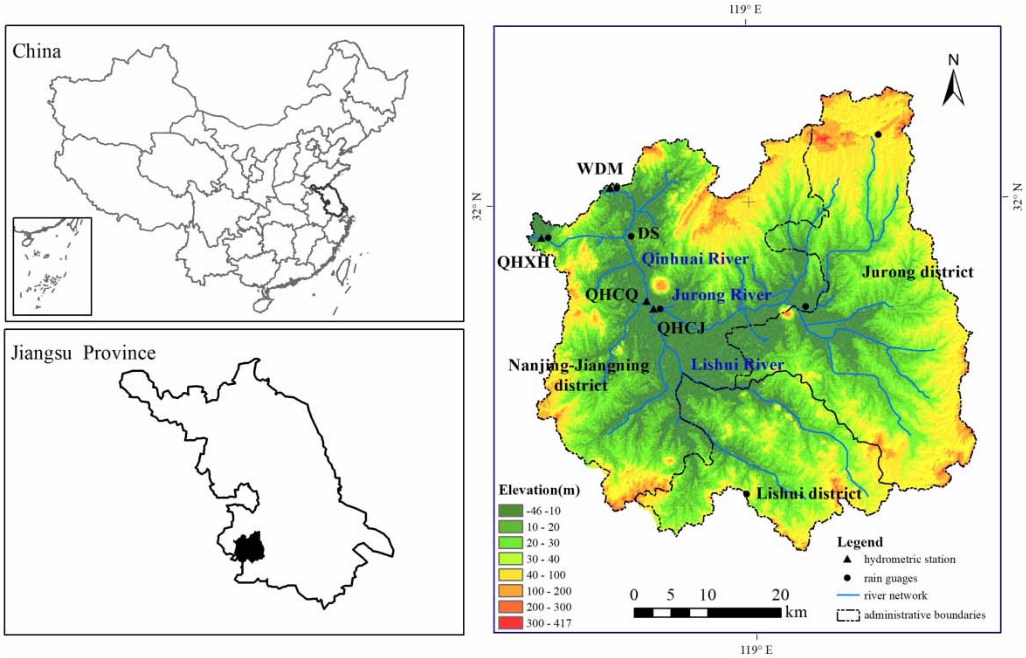

Figure 1 | River system of the Qinhuai River and locations of rain gauges and hydrological stations.

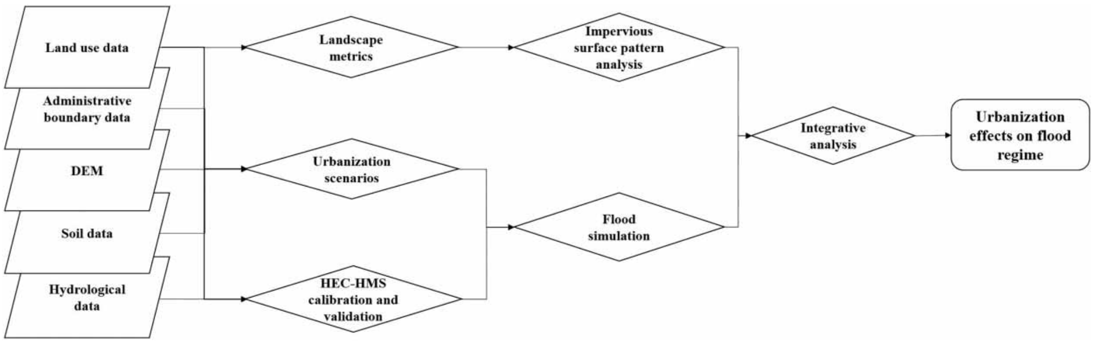

Figure 2 | Framework of hydrological response to changes in TIA.

a classifier ensemble system proposed by Rodríguez *et al.* (2006), was applied to extract impervious surface information. The overall accuracy (OA) and Kappa coefficient of land-use information were above 0.9 and 0.83.

Metrics of impervious area pattern

Five class-level metrics that evaluated different aspects of urban development patterns were calculated by *Fragstat*s (Mcgarigal 2014). The ecological implications of landscape pattern metrics are shown in Table 1.

Construction of urban scenarios

Urban scenarios construction was based on land-use data for four years: 1994, 2003, 2009 and 2013. It was derived from Landsat image interpretation and represented different stages of urbanization (Figure 3).

Table 1 | Formulas and ecological implications of landscape pattern metrics (Mcgarigal 2014)

Landscape pattern metrics	Formula	Technical description
Impervious surface ratio	$\frac{ISA}{TA}(100)$	ISA is the impervious surface area, TA is the total area
Number of patches (NP)	n_k	NP is used to describe the heterogeneity of landscape. n_k is the patch number of land use k
Mean patch size (MPS)	$\frac{A}{n_k} \times 10^6$	The ratio of the total area (A) of land use k to the number of patches. MPS represents an average situation
Maximum patch size (LPI)	$\frac{\max(a_i j)}{A}(100)$	$0 \le \text{LPI} \le 100$, a_{ij} is the area of patch in row i, column j. This index determines the dominant species of the landscape
Landscape shape index (LSI)	$\frac{0.25E}{\sqrt{A}}$	E is the total patch length, and LSI = 1 when there is only one square patch. The more irregular the shape, the larger the LSI
Aggregation index (AI)	$\left[\frac{g_{ij}}{\max \to g_{ij}}\right](100)$	g_{ij} is the length of common boundary between the same type of patches. When common boundary reaches the maximum, it has the maximum aggregation index

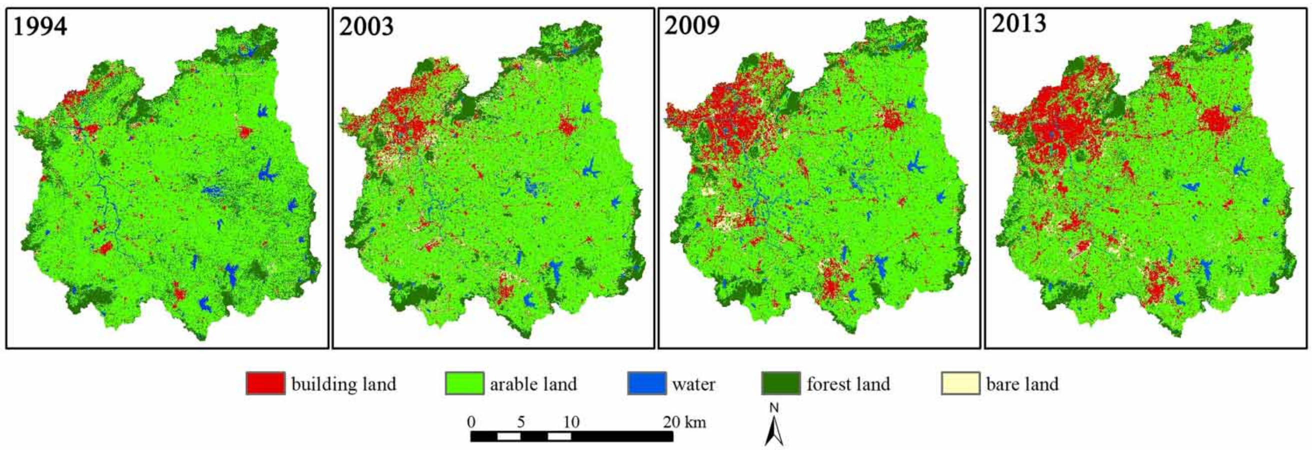

Figure 3 | Land-uses over the Qinhuai River basin in four typical years (1994, 2003, 2009, and 2013).

The basin was divided into three hydrological response districts: Nanjing-Jiangning (NJ + JN) district, Lishui (LS) district and Jurong (JR) district. Ten urban landscape scenarios were hypothesized by making one of these districts' urban landscape data change from 1994, 2003, 2009 to 2013 in turn, with other districts' remaining in 1994. Three urban area expansion patterns were simulated based on the 10 scenarios. Urban area expansion pattern 1 is composed of scenario 1, scenario 2, scenario 3 and scenario 4. It means urbanization expansion only occurred in NJ + JN district from 1994 to 2013. Urban area expansion pattern 2 is composed of scenario 1, scenario 5, scenario 6 and scenario 7. It means urbanization expansion only occurred in LS district from 1994 to 2013. Urban area expansion pattern 3 is composed of scenario 1, scenario 8, scenario 9 and scenario 10. It means urbanization expansion only occurred in JR district from 1994 to 2013. The impacts of different urbanization relative locations on the flood regime were analyzed through flood simulation based on the 10 scenarios. The hydrological response districts in the Qinhuai River basin and the landscape configuration scenarios are shown in Figure 4.

HEC-HMS model description

The HEC-HMS model consists of the basin model, the meteorological model and control specifications. The model uses separate sub-models to calculate the rainfall

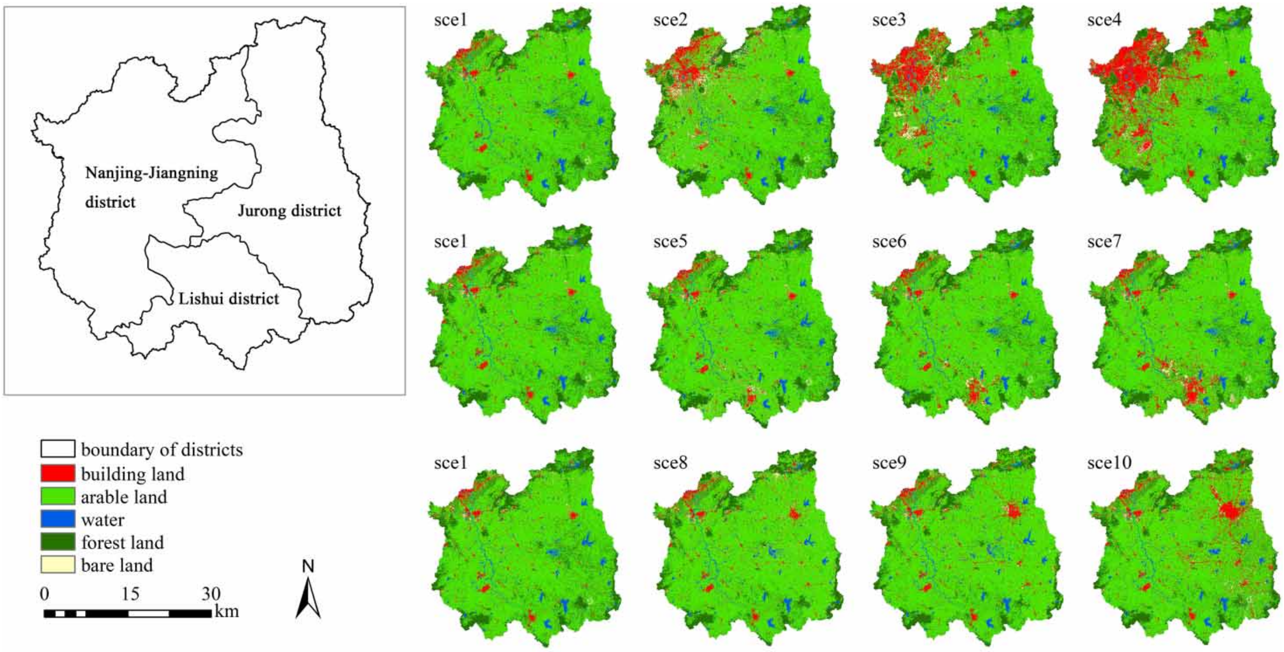

Figure 4 | Hydrological response districts of the Qinhuai River basin and the 10 landscape scenarios.

losses, runoff generation and base flow. The separate sub-models are connected by the channel routing model. The basin model contains the parameters related to the runoff process of sub-models and the routing model. The meteorological model contains the rainfall input data. Users define the calculation step length and other time information through the control specifications module.

The net rainfall was calculated based on the SCS Curve Number method (Singh 1994; Mishra & Singh 2003), which can be calculated by:

$$P_e = \frac{(P - 0.2S)^2}{P + 0.8S} \tag{1}$$

where P_e is the cumulative net rainfall of sub-basin i at time t; P is the depth of rainfall at time t; S is the potential maximum interception, which is the measure of the basin absorbing and intercepting stormy rainfall. Before the cumulative net rainfall exceeds the initial rainfall loss, both the net rainfall and the rainfall equal to zero. Then, the increment of net rainfall equals the difference value of the cumulative net rainfall at the beginning and in the end.

The maximum retention S and basin characteristics are related through an intermediate parameter, the curve number (commonly abbreviated CN) as:

$$S = \frac{25400 - 254\mathrm{CN}}{\mathrm{CN}} \tag{2}$$

The CN for a basin can be estimated as a function of land use, soil type, and antecedent basin moisture, using tables published by SCS (USACE-HEC 2008).

The Snyder unit hydrograph (SUH) model was used to simulate the process of direct runoff of excess precipitation on a basin. The model provides relationships for estimating the SUH parameters from basin characteristics. Two parameters should be defined: basin lag T_p and SUH peaking coefficient C_p. An exponential formula is used to estimate T_p:

$$T_p = 26n\left(\frac{LL_c}{S^{0.5}}\right)^{0.33} \tag{3}$$

S is the scope of study area, feet/mile; L is the length of main stream; L_c is the length along the main stream from the outlet to a point nearest the basin centroid; $_n$ is basin coefficient which is the function of impervious rate and land use. The referenced values of the basin coefficient are shown in Table 2 (USACE-HEC 2008):

SUH peak coefficient C_p relates to the sharpness degree of unit hydrograph which is somewhere between 0.4 and 0.8. C_p can be estimated based on the peak flow of known unit hydrograph (Sun & Wang 1993):

$$C_p = \frac{Q_p T_p}{640A} \tag{4}$$

where Q_p is the peak value of standard unit hydrograph in cubic feet/second. A is the drainage area (square miles).

A recession model was applied to simulate the channel flow receding exponentially after an event. Initial discharge, recession constant and ratio to peak were needed to calculate the receding limb of the hydrograph (Linsley *et al.* 1982).

The Muskingum model was applied to estimate the channel flow. There are two critical parameters in this model: K refers to the travel time of the flood wave through routing reach while X refers to dimensionless weight and decides the reduction amount of flood at the reach, which is between 0 and 0.5 (Linsley *et al.* 1982).

Model calibration and verification

The basin is divided into 18 sub-catchments based on the digital elevation model (DEM), soil map and land-use data. The rainfall data of 18 sub-catchments were obtained by the Tyson polygon method based on hourly rainfall data of 14 storm events at seven rain gauges. The observed runoff data of 14 storm events is from four hydrometric stations: QHCJ, QHXQ, QHXH, WDM. The location of the hydrometric stations is shown in Figure 1. The scope of two upper stream tributaries – the JR tributary and the LS tributary – were calibrated based on records from the QHCJ and QHCQ stations. The two basin outlets are monitored by the QHXH and WDM stations separately. So the series data from the two hydrometric stations were summed up based on time series to represent the data of the total basin (TB) outlet. Then the remaining scope of the basin was calibrated using the total basin outlet data. The upper and lower reaches were calibrated in turn in order to improve the model accuracy.

Three evaluation indexes were used in model calibration and validation: the Nash coefficient (Nash & Sutcliffe 1970), relative peak flow error and relative peak volume error. The relative error refers to the ratio of the simulation value to the observation value, expressed as a percentage.

The model parameters were calibrated by empirical formula and manual optimization. The 18 sub-catchments are characterized by different geomorphic features, soil types and land-use patterns. These parameters of each sub-catchment are related to the factors that can reflect the physical characteristics and land use of the basin through empirical formulas (USACE-HEC 2008). It is worth noting that CN in the SCS CN model, and T_p and C_p in the Snyder unit hydrograph are the most sensitive parameters in model calibration. CN can be estimated as a function of land use, soil type, and antecedent basin moisture. Basin lag T_{p} and SUH peaking coefficient C_{p} are both key factors of the hydrograph, determining the peak flow time and flood peak value. They are all sensitive to the imperviousness expansion. It is difficult to achieve satisfactory results using one set of fixed values. The final values of each sub-catchment were determined by means of optimal coefficients. Four groups of parameters based on various impervious surface levels were applied to calibrate and validate the model. Fourteen flood events were matched to the land-use data by the nearest year. The land-use data and flood event combination for calibration and validation are shown in Table 3.

Table 2 | Reference table of basin coefficient *n*

	n	
Land use	**Developed area**	**Undeveloped area**
Business zone	0.031	0.070
Residential area: 4–6 buildings/acre	0.042	0.084
Residential area: 3–4 buildings/acre	0.046	0.088

RESULTS AND DISCUSSION

Changes in TIA and spatial pattern

TIA is quantified by the impervious surface ratio. This ratio increased significantly in the Qinhuai River basin, from

Table 3 | Modeling methodology.

Land use	Storm events	Stage
1994	19870702	Calibration
	19910612	Validation
2003	20030630	Calibration
	20060719	Validation
2009	20080801	Calibration
	20090706	Calibration
	20090721	Validation
	20100712	Validation
2013	20110624	Calibration
	20110715	Calibration
	20120713	Calibration
	20120808	Validation
	20130705	Validation
	20140701	Validation

3.92% in 1994 to 17.48% in 2013, with average annual growth of 6.04%. There were spatial and temporal variations in TIA over the 20 years. The urban area in NJ + JN district had the highest water permeability and increased from 4.4 to 30.9%. LS district was second, rising sharply from 2.9 to 15.2%. JR had the lowest urbanization level, where the impervious surface ratio had increased from 3.8 to 12.7%. All three districts showed a more remarkable increase in the second decade than in the first. The impervious surface ratios are shown in Figure 5.

According to the pattern metrics results, the impervious surface pattern also showed spatial and temporal differences between the former and the latter stage. NP is a key indicator of landscape connectivity and combining analysis of TIA with NP is a good method to evaluate land-use configuration. Specifically, if new patches and existing patches of impervious surface do not connect, the number of patches thereupon increases. However, if new patches extend based on existing patches and connect to each other, the number of patches remains unchanged or even decreases as the area increases. The TIA in the Qinhuai River basin continued to increase during the 20 years, while NP grew accordingly and decreased in the latter stage. Urban landscape configurations were more concentrated in the latter period of urbanization. NJ + JN district showed the most obvious increasing trend in TIA and decreasing trend in NP.

In addition, there is a simultaneous trend in MPS, LPI, LSI and AI. While the new patches of impervious surface grew significantly during 1994 to 2003, the patch density increased accordingly and the shape of impervious surface patches tended to be scattered and disorderly. In the latter stage in 2003–2013, the patch density remained stable and the shape of impervious patches became more regular and complete. Among the three districts, NJ + JN district had the highest level of agglomeration structure.

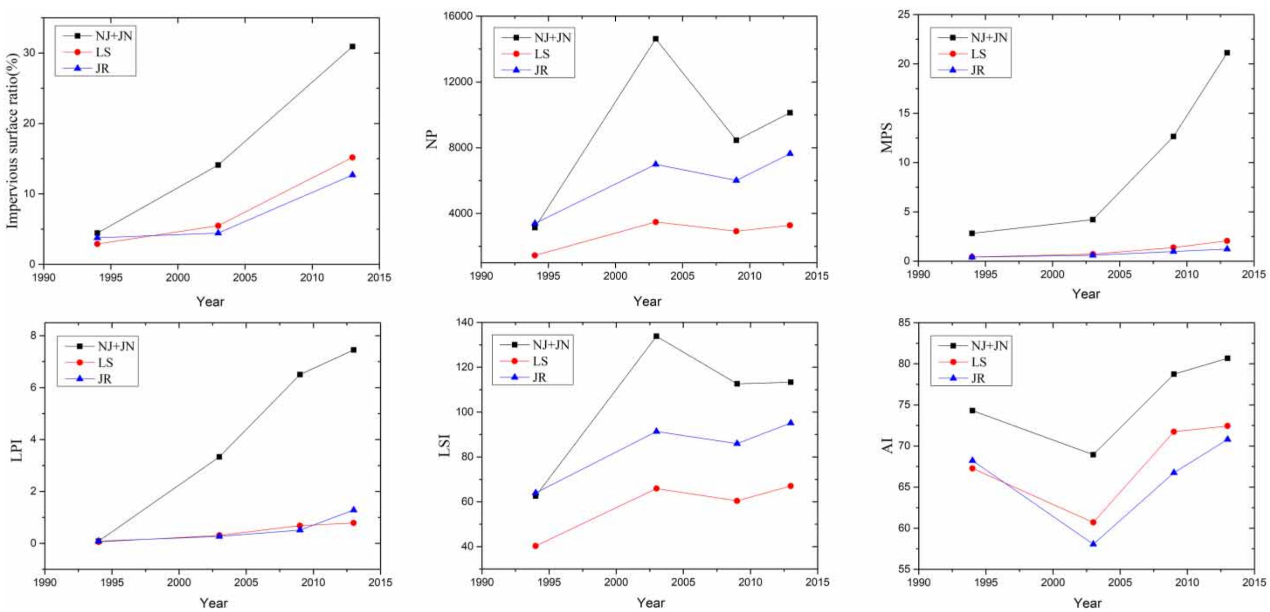

Figure 5 | Total impervious surface ratio (%) and landscape pattern metrics of TIA.

Calibration and validation results of the HEC-HMS model

The model validation results showed that the average Nash coefficient (NSE) in the QHCQ hydrometric station and TB outlet were 0.82 and 0.85. Observed peak flow, relative peak flow error, relative peak volume error are shown in Table 4 and abbreviated as Peak Q obs, D_p, D_v. These results showed that the model performance was satisfactory during both the calibration and validation periods. The HEC-HMS model was applicable for quantifying the effects of urbanization on flood regimes. The observed and simulated hydrographs of 14 flood events are shown in Figure 6.

The three sensitive parameters calibrated values are shown in Table 5.

Impacts of TIA magnitude on flood regimes

Using the rainfall data of 14 storm events and the four sets of model parameters calculated by the land use data of 1994, 2003, 2009 and 2013, hydrographs of the 14 flood events under the four different TIA magnitudes were simulated and are shown in Figure 7.

The flood hydrographs in the river basin generally showed the trend of increasing height, becoming sharp and becoming thin on the premise of increasing water permeability. Peak discharge and volume changes of 14 floods based on land-use data in 1994, 2003, 2009, 2013 are shown in Figure 8. Peak flow increased significantly by an average increase degree of 80% and flood volume increased by an average increase degree of 37% while the impervious ratio grew from 4.43% in 1994 to 17.48% in 2013. The increasing impervious surface made the natural half-underground runoff pattern convert to over-ground flow on a large scale, which cut the base flow volume substantially. Flood peak flow showed a more sensitive increasing trend than flood volume when the impervious area expanded. The influence of the variation of underlying surface on flood regimes was mainly to change the time distribution of the flood hydrograph.

Flood response to different magnitudes of storms

Based on the simulation results of the flood events on the premise of 1994 land use, the 14 flood events were divided into two orders according to the peak flow magnitudes. Flood events with a peak flow higher than 700 m^3 per

Table 4 | Results of calibration and validation in the QHCQ station and total basin

	Station: QHCQ				Station: TB			
Event	**Peak Q Obs**	**NSE**	**Dp**	**Dv**	**Peak Q Obs**	**NSE**	**Dp**	**Dv**
19870702	731	0.82	−7.54	25.32	880	0.90	−9.27	11.08
19910612	964	0.78	16.08	3.35	1280	0.94	9.81	−7.96
20030630	–	–	–	–	1090	0.87	23.08	12.23
20060719	513	0.74	−2.75	13.21	595	0.80	2.99	1.69
20080801	654	0.88	1.67	22.56	1045	0.84	−22.68	5.95
20090706	779	0.87	−1.80	21.77	900	0.81	−2.40	8.03
20090721	775	0.83	12.61	22.96	1025	0.82	14.24	25.10
20100712	491	0.64	14.68	28.60	647	0.83	0.49	14.74
20110624	588	0.86	−4.51	0.54	769	0.86	−12.42	−5.64
20110715	517	0.87	21.18	4.55	820	0.84	−11.07	−22.52
20120713	380	0.79	−1.34	14.86	503	0.86	−8.91	7.38
20120808	667	0.87	0.00	2.35	775	0.87	13.42	0.66
20130705	497	0.85	2.33	8.17	697	0.84	−14.31	−4.28
20140701	772	0.88	7.03	2.59	875	0.82	5.87	−8.19

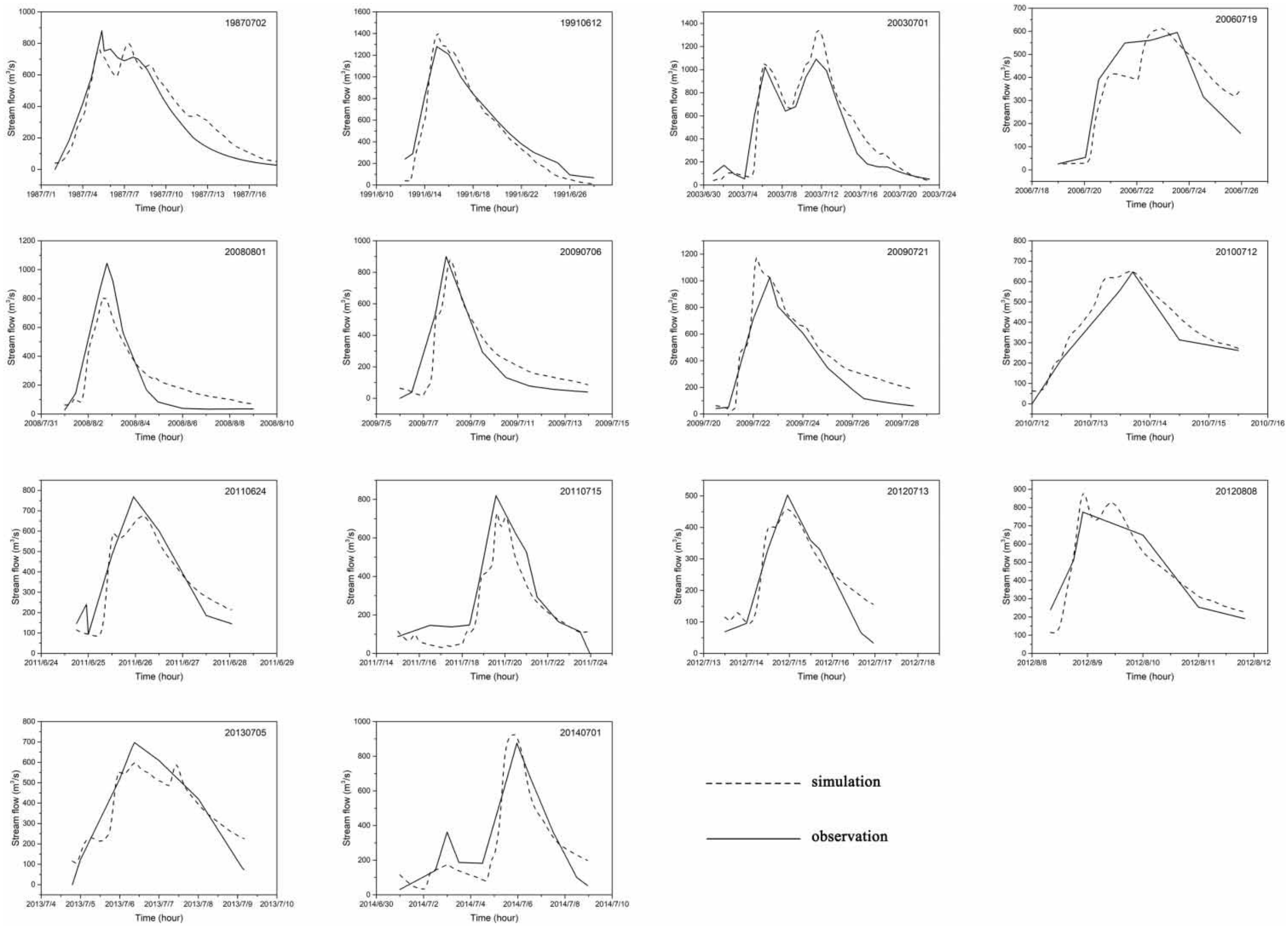

Figure 6 | Simulated and observed hydrographs of 14 flood events.

second were classified as major floods and those with a peak flow lower than 700 m^3 per second were classified as minor floods.

During the two decades, the average peak flow growth rate of major floods according to the urbanization expansion was 49%, while the rate for small floods was 90%. The average volume growth rate of major floods according to the urbanization expansion was 13, and 42% for small floods (Figure 9). The reason for this difference is that a rural catchment may become so saturated and its channel network so extended during severe and prolonged rainstorms. It responds hydrologically as if it were an impervious catchment with a dense network of surface water drains and so it produces floods of a type and size similar to those of its urban counterpart.

Impacts of TIA location on flood regime

The relative contribution of urbanization expansion in different hydrological units in the basin were analyzed according to the simulation results of 14 flood events based on 10 land-use scenarios. The 10 land-use scenarios represented three different urban area expansion patterns. The peak discharges of these scenarios are shown in Figure 10. Pattern 3, which represents the regional expansion of urbanization only occurred in JR district: scenario 1, scenario 8, scenario 9 and scenario 10, showed the highest growth rate in peak discharge among the three patterns.

The contribution rate of urban area expansion was evaluated for each of the three units by calculating the weight of flood peak increment by urban growth in each unit to flood

Table 5 | Calibrated sub-catchment parameters

	1994 Land use			2003 Land use			2009 Land use			2013 Land use		
Sub-basin	CN	T_p	C_p	CN	T_p	C_p	CN	T_p	C_p	CN	T_p	C_p
sub1	72.27	13.82	0.10	72.42	13.87	0.11	74.04	13.82	0.20	74.85	13.83	0.23
sub2	80.27	10.88	0.10	80.30	10.99	0.13	81.09	10.88	0.38	80.63	10.88	0.42
sub3	83.51	9.14	0.10	84.13	9.26	0.12	84.62	9.14	0.13	83.92	9.03	0.16
sub4	77.46	1.00	0.10	79.63	3.48	0.16	78.34	3.34	0.54	76.13	3.11	0.10
sub5	81.50	1.00	0.10	84.85	6.54	0.13	87.28	6.32	0.21	86.56	3.90	0.21
sub6	78.17	9.56	0.10	79.82	10.18	0.12	80.49	3.00	0.12	80.22	8.94	0.61
sub7	86.22	6.32	0.10	87.05	6.65	0.13	85.89	3.00	0.15	84.66	4.11	0.74
sub8	84.39	12.52	0.10	84.24	12.71	0.12	84.73	12.81	0.10	84.28	12.43	0.12
sub9	86.07	14.37	0.10	85.70	14.58	0.12	86.30	14.62	0.11	86.06	14.34	0.13
sub10	83.94	3.00	0.10	83.99	3.01	0.13	83.76	3.01	0.10	84.13	2.98	0.20
sub11	84.91	16.92	0.10	85.20	17.19	0.12	85.59	17.36	0.10	85.91	16.67	0.12
sub12	86.36	8.79	0.10	86.53	8.83	0.15	87.14	8.87	0.10	86.81	8.73	0.38
sub13	73.90	10.83	0.10	74.34	10.88	0.11	76.29	10.91	0.28	75.67	10.81	0.22
sub14	76.12	7.81	0.10	76.28	7.83	0.12	77.07	7.85	0.25	76.55	7.77	0.26
sub15	78.64	3.66	0.10	78.43	3.67	0.12	78.93	3.67	0.34	77.59	3.66	0.35
sub16	81.24	6.32	0.10	80.90	6.35	0.14	81.30	6.38	0.66	80.57	6.31	0.69
sub17	80.07	14.03	0.10	80.43	14.30	0.11	80.56	14.54	0.20	80.12	13.86	0.23
sub18	85.79	16.41	0.10	86.07	16.44	0.12	86.22	16.55	0.13	85.40	16.32	0.15

peak increment caused by urban growth in the whole basin. The results are shown in Table 6.

The impervious surface rates of NJ + JN district in 1994 and 2013 were 7.18 and 29.99% respectively. The absolute increment and relative growth rates were 191.34 km^2 and 317.53% respectively. All three of the impervious area indicators of NJ + JN district were the highest among the three hydrological units and the impervious area in NJ + JN district presented the highest connectivity and degree of aggregation. The contribution of this district to the total basin peak flow was 16%. However, the impervious surface rates of JR in 1994 and 2013 were both low. The absolute increment of impervious area was 96.88 km^2, which was far less than NJ + JN district. The relative growth rate of TIA was slightly lower than NJ + JN district. However, the contribution of urban growth in JR district to the total basin peak flow was 69%, which was the highest in the whole basin.

The distribution of impermeable surface is one of the factors influencing the flood effects of urbanization and has been examined in several studies. Anderson (1970) estimated the flood hydrographs for drainage basins with various degrees of urban or suburban development based on uniform landscape distribution. They also found that if urbanization occurred in the lower or upper part of the basin, very different hydrographs may result. Hammer (1972) explored the differences between the channel enlargement effects of different impervious land uses, finding that the relative importance of the various topographic and drainage system characteristics is difficult to establish, but the slope factors appear to be more influential than distance factors that involve the location of development within the watershed. Gao et al. (2017) simulated flood hydrographs with different urban agglomeration polders type of flood control pattern and concluded that the distribution of the city circle polder had no obvious impact on flood volume, but has an effect on peak flow. The results in this study pointed to the same conclusion.

Urban areas that are distributed in upper parts of the basin have more significant impacts on flood peaks in

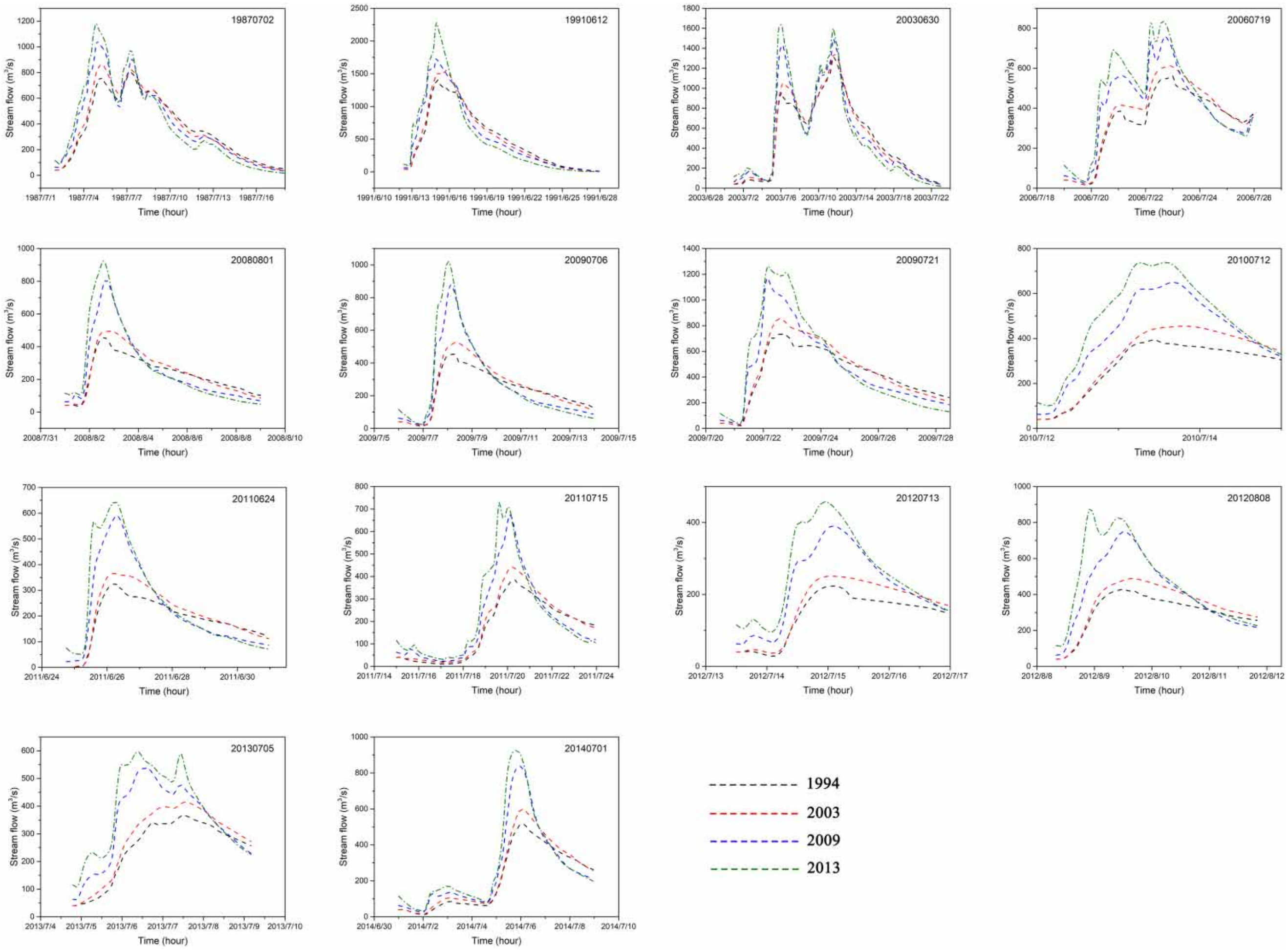

Figure 7 | Flood hydrographs under four TIA magnitudes.

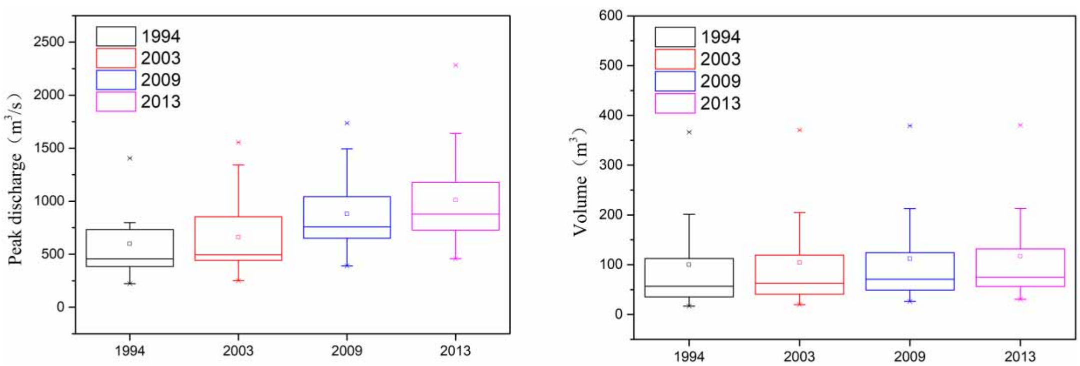

Figure 8 | Peak discharge and volume with different land cover.

basin outlets than those in lower parts. The upper areas with a certain hydraulic transmission distance can have a great contribution to the total flood peak while the flood runoff generated in lower areas flows quickly out of the basin. Besides, the flood effects vary among different basin shapes. Fan-shaped basins have a steeper hydrological

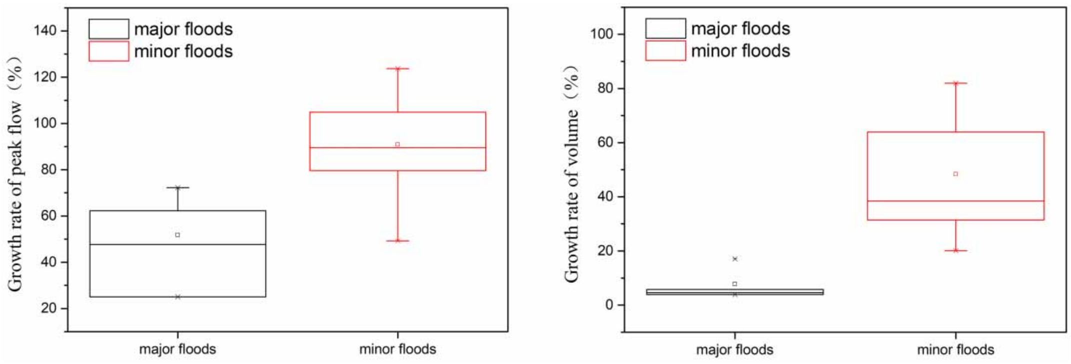

Figure 9 | Peak discharge and volume growth rates of different flood magnitudes.

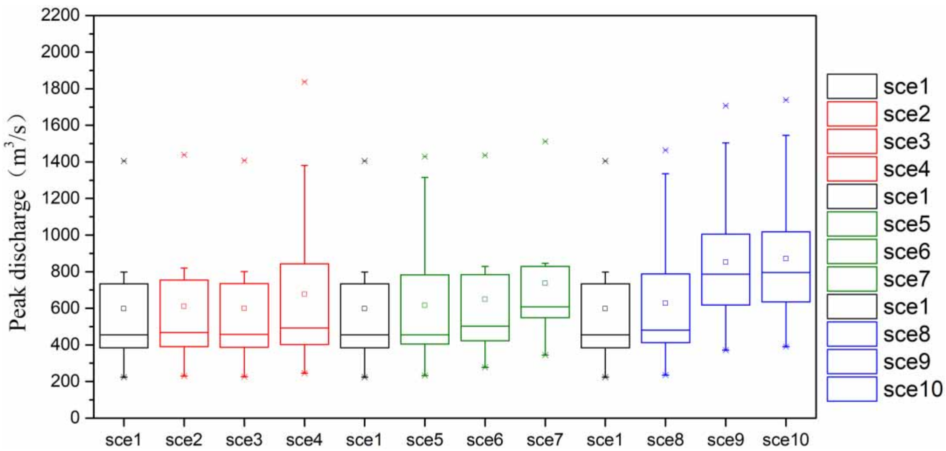

Figure 10 | Peak discharge of 14 floods based on 10 scenarios.

hydrograph because the farther up the stream in the basin can lead to larger areas with the same hydraulic transmission distance. Thus, urbanization that expands in upper areas in a fan-shaped basin can have a more significant contribution to the flood peak discharge in the total basin.

Correlations between flood characteristics and urban development patterns

To identify the aspects of flood regimes that are influenced by urban development patterns, correlation coefficients were calculated between the flood characteristic indexes and landscape metrics, as shown in Table 7. Six landscape pattern metrics of TIA, arable land, forest land were generated by 10 land-use scenarios. Based on the simulation results of 14 flood events under 10 land-use scenarios, three flood regime characteristic indexes – average value of peak flow (Mean), standard deviation of peak flow (STDEV), coefficient of variation of peak flow (CV) – were calculated (Table 7).

The area mean patch size (MPS), maximum patch size (LPI) and aggregation index (AI) of TIA showed significant positive correlations with the standard deviation of flood peak flow (STDEV). The larger area and aggregation extent of TIA will lead to a greater impact of urbanization on the hydrologic cycle. The rapid expansion of impermeable surfaces weakened the natural flood regulation and storage function of the basin. It intensified the dispersion and extremes of the flood peak value, reducing the stability of the hydrologic cycle. The landscape pattern metrics of arable land displayed a strong correlation with flood peak coefficient of variation (CV). The area, MPS, LPI and AI

Table 6 | Contribution rates of urbanization in three units to total basin growth in peak discharge

	Peak growth with land use varies from 1994 to 2013 (m^3/s)				Contribution rate (%)		
Flood events	**Total basin**	**NJ + JN**	**LS**	**JR**	**NJ + JN**	**LS**	**JR**
19870702	381	44	47	219	12	12	57
19910612	876	431	106	333	49	12	38
20030630	328	69	57	234	21	17	71
20060719	277	51	173	233	18	62	84
20080801	469	41	152	366	9	33	78
20090706	565	36	160	444	6	28	79
20090721	530	201	96	314	38	18	59
20100712	345	40	100	243	11	29	70
20110624	343	36	218	257	10	64	75
20110715	344	18	176	250	5	51	73
20120713	234	22	121	167	9	51	71
20120808	451	53	367	301	12	81	67
20130705	229	33	135	148	14	59	64
20140701	411	37	36	331	9	9	80

of arable land are negatively correlated to CV. This relationship indicates that large and lumped arable land can enhance the flood storage function of the basin and weaken the dispersion and extremes of the flood peak value. The forest land area displayed the strongest correlation with the average value of peak flow (mean). Forest land has a stronger storage capacity than arable land. Increasing forest land area has a significant effect on reducing flood peaks. Compared to the impervious surface, forest land and arable land showed an opposite effect on the basin water cycle.

CONCLUSIONS

This study investigated how patterns of imperviousness affect flood regimes. The impervious surface patterns were evaluated by three indicators: TIA, landscape configuration and relative location in the basin. Flood hydrographs were calculated by a distributed hydrological model HEC-HMS, which was adapted to the large-scale basin with two basin outlets. The model was calibrated and validated according to the drainage characteristics and land-use information based on 14 flood events. Four groups of parameters were used to simulate flood hydrographs based on different land-use conditions.

The results showed that the landscape pattern had changed significantly. Overall, the impervious area had increased by nearly four times. The dominance of impervious surfaces had increased greatly and the turning point of urban expansion was 2003. Urban expansion mainly occurred in NJ + JN district before the turning point, while the impervious surface expansion rate of NJ + JN district decreased after that. At the same time, there was a sharp rise in the expansion rate of LS and JR. The impervious surface had the highest spatial heterogeneity in 2003, and then decreased significantly from that time point to 2013. The shape of the impervious patches became simpler at the latter stage, and the impervious surface turned from dispersed distribution

Table 7 | Correlation coefficient between landscape pattern metrics and flood characteristics

	TIA				Arable land				Forest land		
Metrics	**Mean**	**STDEV**	**CV**	**Metrics**	**Mean**	**STDEV**	**CV**	**Metrics**	**Mean**	**STDEV**	**CV**
Area	–0.06	0.71*	0.43	Area	0.49	–0.46	–0.69*	Area	–0.83**	–0.21	0.63
NP	0.00	0.11	0.07	NP	–0.56	0.38	0.71*	NP	–0.57	0.00	0.52
MPS	–0.07	0.66*	0.41	MPS	0.64	–0.29	–0.73*	MPS	–0.23	–0.34	0.01
LPI	–0.22	0.64*	0.54	LPI	0.49	–0.42	–0.68*	LPI	0.18	–0.56	–0.46
LSI	0.04	–0.27	–0.17	LSI	–0.63	0.24	0.70*	LSI	–0.54	–0.05	0.46
AI	0.04	0.64	0.31	AI	0.60	–0.30	–0.71*	AI	0.15	–0.12	–0.20

Note: *indicates a significant correlation at confidence level of 0.05.
**indicates a significant correlation at confidence level of 0.01.

to higher connectivity. Besides, the area with high level of connectivity was mainly distributed at the NJ + JN district.

The accuracy of the HEC-HMS model was improved effectively, with the Nash coefficient above 0.8. The flood hydrographs generally showed the trend of increasing height, becoming sharp and thin on the basis of increasing water permeability. Peak flow increased significantly by an average increase degree of 80% when impervious ratio grew from 4.43% in 1994 to 17.48% in 2013. During the period of 1994–2013, the average peak flow growth rate of major floods to urbanization expansion was 49%, while the rate for small floods was 90%. The imperviousness rates of JR in 1994 and 2013 were both low, but the contribution of JR to the total basin peak flow was 69%, which was the highest for the whole basin.

The area, MPS, LPI and AI of TIA displayed significant positive correlations with the standard deviation of flood peak flow. The area, MPS, LPI and AI of arable land are negatively correlated to the flood peak coefficient of variation. The forest land area displayed the strongest correlation with average value of peak flow. Compared to the impervious surface, forest land and arable land showed an opposite effect on the basin water cycle.

The results of this study can provide useful ideas and insights for land-use planners and managers. JR and LS have been urbanized rapidly in recent years and they are both distributed in the inner basin. With the increasing level of urbanization, the connectivity of the impervious areas in this region will be gradually enhanced, and the water confluence characteristics of the basin's fan-shape will bring more significant flood control pressure to the outlet of the basin, the main urban area of Nanjing.

ACKNOWLEDGEMENTS

This work was supported by the National Natural Science Foundation of China through the project (Grant Nos. 51879162,41830863), the National Key Research and Development Programs of China (Grants: 2016YFA0601501), and the Belt and Road Fund on Water and Sustainability of the State Key Laboratory of Hydrology-Water Resources and Hydraulic Engineering (Grant No. 2019nkzd02). The authors acknowledge the anonymous reviewers for their insightful comments and suggestions. The authors thank the late Jinkang Du, professor from Nanjing University, who is greatly missed, for his constructive guidance and comments.

DATA AVAILABILITY STATEMENT

All relevant data are included in the paper or its Supplementary Information.

REFERENCES

Alberti, M., Booth, D., Hill, K., Coburn, B., Avolio, C., Coe, S. & Spirandelli, D. 2007 The impact of urban patterns on aquatic ecosystems: an empirical analysis in Puget lowland sub-basins. *Landsc. Urban Plan.* **80** (4), 345–361.

Anderson, D. G. 1970 *Water in the urban environment: effects of urban development on floods in Northern Virginia*. U.S Geological Survey Water Supply Paper. 2001-C, 22 pp.

Arnold, C. L. & Gibbons, C. J. 1996 Impervious surface coverage: the emergence of a key environmental indicator. *J. Am. Plan. Assoc.* **62** (2), 243–258.

Blum, A. G., Ferraro, P. J., Archfield, S. A. & Ryberg, K. R. 2020 Causal effect of impervious cover on annual flood magnitude for the United States. *Geophys. Res. Lett.* **47** (5). doi:10.1029/2019GL086480

Chen, Y., Xu, Y. & Yin, Y. 2009 Impacts of land use change scenarios on storm-runoff generation in Xitiaoxi basin, China. *Quat. Int.* **208** (1–2), 121–128. doi:10.1016/j.quaint.2008.12.014.

Chen, J., Theller, L., Gitau, M. W., Engel, B. A. & Harbor, J. M. 2016 Urbanization impacts on surface runoff of the contiguous United States. *J. Environ. Manage.* **187** (1), 470–481.

Cheng, S. J. & Wang, R. Y. 2002 An approach for evaluating the hydrological effects of urbanization and its application. *Hydrol. Process.* **16** (7), 1403–1418.

Dadashpoor, H., Azizi, P. & Moghadasi, M. 2019 Land use change, urbanization, and change in landscape pattern in a metropolitan area. *Sci. Total Environ.* **655**, 707–719.

Debbage, N. & Shepherd, J. M. 2018 The influence of urban development patterns on streamflow characteristics in the charlanta megaregion. *Water Resour. Res.* **54** (5), 3728–3747.

Defries, R. & Eshleman, K. N. 2004 Land-use change and hydrologic processes: a major focus for the future. *Hydrol. Process.* **18** (11), 2183–2186.

Du, J., Qian, L., Rui, H., Zuo, T., Zheng, D., Xu, Y. & Xu, C. Y. 2012 Assessing the effects of urbanization on annual runoff and flood events using an integrated hydrological modeling system for Qinhuai River basin, China. *J. Hydrol.* **464–465** (5), 127–139.

Fu, P. & Weng, Q. 2016 A time series analysis of urbanization induced land use and land cover change and its impact on land surface temperature with landsat imagery. *Remote Sens. Environ.* **175** (4), 205–214.

Gao, Y., Yuan, Y., Wang, H., Schmidt, A. R., Wang, K. & Ye, L. 2017 Examining the effects of urban agglomeration polders on flood events in Qinhuai River basin, China with HEC-HMS model. *Water Sci. Technol.* **75** (9), 2130–2138.

Hall, J., Arheimer, B., Borga, M., Brázdil, R., Claps, P., Kiss, A. & Blöschl, G. 2014 Understanding flood regime changes in Europe: a state-of-the-art assessment. *Hydrol. Earth Syst. Sci.* **18** (7), 2735–2772. doi:10.5194/hess-18-2735-2014.

Hammer, T. R. 1972 Stream channel enlargement due to urbanization. *Water Resour. Res.* **8**, 1530–1540.

Hollis, G. E. 1975 The effect of urbanization on floods of different recurrence interval. *Water Resour. Res.* **11** (3), 431–435.

Jiang, S., Ren, L., Yong, B., Singh, V. P., Yang, X. & Yuan, F. 2011 Quantifying the effects of climate variability and human activities on runoff from the Laohahe basin in northern China using three different methods. *Hydrol. Process.* **25** (16), 2492–2505. doi:10.1002/hyp.8002.

Kim, H. W. & Park, Y. 2016 Urban green infrastructure and local flooding: the impact of landscape patterns on peak runoff in four Texas MSAs. *Appl. Geogr.* **77**, 72–81.

Knebl, M. R., Yang, Z. L., Hutchison, K. & Maidment, D. R. 2005 Regional scale flood modeling using NEXRAD rainfall, GIS, and HEC-HMS/RAS: a case study for the San Antonio River basin summer 2002 storm event. *J. Environ. Manage.* **75** (4), 325–336. doi:10.1016/j.jenvman.2004.11.024.

Konrad, C. P. & Booth, D. B. 2005 Hydrologic changes in urban streams and their ecological significance. *Am. Fish. Soc. Symp.* **47**, 157–177.

Lee, J. G. & Heaney, J. P. 2003 Estimation of urban imperviousness and its impacts on storm water systems. *J. Water Resour. Plan. Manage.* **129** (5), 419–426.

Linsley, R. K., Kohler, M. A. & Paulhus, J. L. H. 1982 *Hydrology for Engineers*. McGraw-Hill, New York.

Mcgarigal, K. 2014 *Landscape Pattern Metrics*. Wiley Online Library, Hoboken, NJ.

Mejia, A. I. & Moglen, G. E. 2010 Impact of the spatial distribution of imperviousness on the hydrologic response of an urbanizing basin. *Hydrol. Process.* **24** (23), 3359–3373.

Mishra, S. K. & Singh, V. P. 2003 *Soil Conservation Service Curve Number (SCS-CN) Methodology*. Springer, Netherlands.

Montanari, G. Y., Savenije, H. H. G., Hughes, D., Wagener, T., Ren, L. L., Koutsoyiannis, D., Cudennec, C., Toth, E., Grimaldi, S., Blöschl, G., Sivapalan, M., Beven, K., Gupta, H., Hipsey, M., Schaefli, B., Arheimer, B., Boegh, E., Schymanski, S. J., Di Baldassarre, G., Yu, B., Hubert, P., Huang, Y., Schumann, A., Post, D. A., Srinivasan, V., Harman, C., Thompson, S., Rogger, M., Viglione, A., McMillan, H., Characklis, G., Pang, Z. & Belyaev, V. 2013 'Panta Rhei – everything flows': change in hydrology and society – The IAHS scientific decade 2013–2022. *Hydrol. Sci. J.* **58** (6), 1256–1275. doi:10.1080/02626667.2013.809088.

Nash, J. E. & Sutcliffe, J. V. 1970 River flow forecasting through conceptual models part I – A discussion of principles. *J. Hydrol.* **10** (3), 282–290.

Oleyiblo, J. O. 2010 Application of HEC-HMS for flood forecasting in Misai and Wan'an catchments in China. *Water Sci. Eng.* **3** (1), 14–22.

Oudin, L., Salavati, B., Furusho-Percot, C., Ribstein, P. & Saadi, M. 2018 Hydrological impacts of urbanization at the catchment scale. *J. Hydrol.* **559**, 774–786.

Poff, L. R., Allan, J. D., Bain, M. B., Karr, J. R., Prestegaard, K. L., Richter, B. D. & Stromberg, J. C. 1997 The natural flow regime: a paradigm for river conservation and restoration. *Bioscience* **47** (11), 769–784.

Rodríguez, J. J., Kuncheva, L. I. & Alonso, C. J. 2006 Rotation forest: a new classifier ensemble method. *IEEE Trans. Pattern Anal. Machine Intell.* **28** (10), 1619–1630.

Schober, B., Hauer, C. & Habersack, H. 2020 Floodplain losses and increasing flood risk in the context of recent historic land use changes and settlement developments: Austrian case studies. *J. Flood Risk Manage.* **2018**, e12610.

Singh, V. P. 1994 *Elementary Hydrology*. Prentice Hall, Englewood Cliffs, NJ.

Sun, S. & Wang, Y. 1993 Study on application of SCS model in Boniuchuan watershed. *Water Resour. Water Eng.* **1**, 28–33.

USACE-HEC 2008 *Hydrologic Modeling System HEC-HMS v3.2 User's Manual*. US Army Corps of Engineers, Hydrologic Engineering Center (HEC), Davis, USA.

Xu, Y., Xu, J., Ding, J., Chen, Y., Yin, Y. & Zhang, X. 2010 Impacts of urbanization on hydrology in the Yangtze river delta, China. *Water Sci. Technol.* **62** (6), 1221–1229.

Zhou, F., Xu, Y., Chen, Y., Xu, C. Y., Gao, Y. & Du, J. 2013 Hydrological response to urbanization at different spatio-temporal scales simulated by coupling of CLUE-S and the SWAT model in the Yangtze river delta region. *J. Hydrol.* **485**, 113–125. doi:10.1016/j.jhydrol.2012.12.040.

First received 29 July 2020; accepted in revised form 3 September 2020. Available online 2 November 2020